ClimateVision V1.2.0

METHODOLOGY

Climate-driven changes in infrastructure design assumptions

February 2026

callendar

Table of content

Disclaimer

The information contained in this document is based on information made available by third parties, subject to continuous change and therefore is not warranted as to their completeness, accuracy or fitness for a particular purpose. Callendar has no obligation to update the information it contains. Accordingly, Callendar, its employees and/or agents accept no responsibility or liability for any loss, damage or expense arising from the use of this report.

For more information see legal and IP notices in Appendix A.

About ClimateVision

Companies engaged in the design and construction of both on- and off-shore infrastructures rely on meteorological and oceanographic assumptions. Variables such as temperature, wind, precipitation, wave height, and sea level play pivotal roles in project feasibility, design, and operation. However, these assumptions, typically grounded in a study of past weather records, may become inadequate over a project's lifetime, especially under the influence of climate change.

ClimateVision is an innovative and efficient solution for accessing future local climate projections crucial for designing resilient infrastructures. Leveraging Callendar's expertise in climatology and data automation, ClimateVision can generate precise local climate projections worldwide in a manner that is both convenient to users and compliant with the current scientific literature.

This document serves as a comprehensive guide to assist ClimateVision users in understanding how their projections are produced. The first chapter, "Overview of Data Sources and Processing", provides a short summary of data sources and processing methodologies for users seeking a broad understanding. The following chapters cover the various methodological elements in full detail for experts and users seeking more complete explanations.

Should you have any further questions on your results, feel free to contact us: contact@callendar.tech.

Overview of data sources and processing of primary indicators

General overview

ClimateVision uses automated data processing to generate climate indicators useful for infrastructure projects from global climate projections. The tool reproduces recognized methodologies using the latest scientific data to produce state-of-the-art local information about current and future climate.

This first part gives a short overview of the data source and methodology used for each indicator.

Average temperature projections

Data

Average temperature projections are based on simulation of future climate by 12 climate models from the Coupled Model Intercomparison Project phase 6 (CMIP6). These projections are a subset of the projections used in the Intergovernmental Panel on Climate Change's 6th assessment report.

The simulation point closest to the location of interest is extracted and the results are downscaled and corrected for bias using historical data from European Centre for Medium-Range Weather Forecasts's reanalysis as reference. ERA5 Land is used for in-land or coastal locations and ERA5 is used on offshore projects.

INDICATOR	PROJECTION	REFERENCE
AVERAGE TEMPERATURE	CMIP6 tas (daily)	ERA5/ERA5 Land t2m (daily average computed from hourly data)

Processing

The impact of climate change for a given decade is then evaluated by averaging corrected projections over 30 years centered on the decade (e.g., average temperature for the decade 2050 is computed based on climate simulations from 2040 to 2069

Average rainfall projections

Data

Average rainfall projections are based on simulation of future climate by 12 climate models from the Coupled Model Intercomparison Project phase 6 (CMIP6). These projections are a subset of the projections used in the Intergovernmental Panel on Climate Change's 6th assessment report.

The simulation point closest to the location of interest is extracted and the results are downscaled and corrected for bias using historical data from European Centre for Medium-Range Weather Forecasts's reanalysis as reference. ERA5 Land is used for in-land or coastal locations and ERA5 is used on offshore projects.

INDICATOR	PROJECTION	REFERENCE
AVERAGE RAINFALL	CMIP6 pr (daily)	ERA5 pr (daily average computed from hourly data)

Processing

Precipitation is processed using a specific correction procedure (see Precipitation special case chapter).

The impact of climate change for a given decade is then evaluated by averaging corrected projections over 30 years centered on the decade (e.g., average temperature for the decade 2050 is computed based on climate simulations from 2040 to 2069).

Average wind speed projections

Data

Average wind projections are based on simulation of future climate by 12 climate models from the Coupled Model Intercomparison Project phase 6 (CMIP6). These projections are a subset of the projections used in the Intergovernmental Panel on Climate Change's 6th assessment report.

The simulation point closest to the location of interest is extracted and the results are downscaled and corrected for bias using historical data from European Centre for Medium-Range Weather Forecasts's reanalysis as reference. ERA5 Land is used for in-land or coastal locations and ERA5 is used on offshore projects.

INDICATOR	PROJECTION	REFERENCE
AVERAGE WIND SPEED	CMIP6 sfcWind (daily)	ERA5/ERA5 Land u10 and v10

		(daily average wind computed from hourly u and v component of wind at 10 meters)

Processing

The corrected wind projections are subsequently used to derive renewable energy indicators.

Average shortwave radiation projections

Data

Average shortwave radiation projections are based on simulation of future climate by 12 climate models from the Coupled Model Intercomparison Project phase 6 (CMIP6). These projections are a subset of the projections used in the Intergovernmental Panel on Climate Change's 6th assessment report.

The simulation point closest to the location of interest is extracted and the results are downscaled and corrected for bias using historical data from European Centre for Medium-Range Weather Forecasts's reanalysis as reference. ERA5 Land is used for in-land or coastal locations and ERA5 is used on offshore projects.

INDICATOR	PROJECTION	REFERENCE
AVERAGE SHORTWAVE RADIATION	CMIP6 rsds (daily)	ERA5/ERA5 Land ssrd (daily average ssrd computed from hourly data)

Processing

The corrected shortwave radiation projections are subsequently used to derive renewable energy indicators.

Extreme temperature projections

Data

Extreme temperature projections are based on simulation of future climate by 12 climate models from the Coupled Model Intercomparison Project phase 6 (CMIP6). These projections are a subset of the projections used in the Intergovernmental Panel on Climate Change's 6th assessment report.

The simulation point closest to the location of interest is extracted and the results are downscaled and corrected for bias using historical data from European Centre for Medium-Range Weather Forecasts's reanalysis as reference. ERA5 Land is used for in-land or coastal locations and ERA5 is used on offshore projects.

INDICATOR	PROJECTION	REFERENCE
MINIMUM TEMPERATURE	CMIP6 tasmin (daily)	ERA5/ERA5 Land t2m (daily minimum computed from hourly data)
MINIMUM DAILY TEMPERATURE	CMIP6 tas (daily)	ERA5/ERA5 Land t2m (daily average computed from hourly data)
MAXIMUM TEMPERATURE	CMIP6 tasmax (daily)	ERA5/ERA5 Land t2m (daily maximum computed from hourly data)
MAXIMUM DAILY TEMPERATURE	CMIP6 tas (daily)	ERA5/ERA5 Land t2m (daily average computed from hourly data)

Processing

Return levels for a selection of return periods are then computed using extreme value analysis.

Extreme rainfall projections

Data

Extreme rainfall projections are based on simulation of future climate by 12 climate models from the Coupled Model Intercomparison Project phase 6 (CMIP6). These projections are a subset of the projections used in the Intergovernmental Panel on Climate Change's 6th assessment report.

The simulation point closest to the location of interest is extracted and the results are downscaled and corrected for bias using historical data from European Centre for

Medium-Range Weather Forecasts's reanalysis as reference. ERA5 Land is used for in-land or coastal locations and ERA5 is used on offshore projects.

INDICATOR	PROJECTION	REFERENCE
MAXIMUM DAILY RAINFALL	CMIP6 pr (daily)	ERA5/ERA5 Land pr (daily average computed from hourly data)

Processing

Precipitation is processed using a specific correction procedure (see Precipitation special case chapter).
Return levels for a selection of return periods are then computed using extreme value analysis.

Extreme wind projections

Data

Extreme wind projections are based on simulation of future climate by 12 climate models from the Coupled Model Intercomparison Project phase 6 (CMIP6). These projections are a subset of the projections used in the Intergovernmental Panel on Climate Change's 6th assessment report.
Since extreme wind speeds must be computed on shorter time steps than those of the climate models, an extrapolation method is used.

The simulation point closest to the location of interest is extracted and the results are downscaled and corrected for bias using historical data from European Centre for Medium-Range Weather Forecasts's reanalysis as reference. ERA5 Land is used for in-land or coastal locations and ERA5 is used on offshore projects.

INDICATOR	PROJECTION	REFERENCE
WIND SPEED	CMIP6 sfcWindmax (daily)	ERA5/ERA5 Land u10 and v10 (daily maximum total wind computed from hourly u and v component of wind at 10 meters)

Extrapolation methodology

ClimateVision provides an evaluation of the local evolution of maximum wind speed over 10 minutes, 1 minute and 3 seconds throughout the 21st century.

Most climate projections are available with monthly, daily, 6-hour or 3-hour time steps. As a result, an extrapolation is necessary to calculate wind speed on a time step of a few minutes to a few seconds from much coarser data. The maximum wind speed for a given return time is then calculated from the downscaled data using the extreme value analysis methods detailed in the previous chapter.

In addition, these projections are typically for sustained wind speeds and do not consider short term phenomena, like gusts. Extreme gusts occur due to a variety of short-lived phenomena that climate models are not designed to capture[i]. The ratio of maximum gust wind speed to mean wind speed can be large[ii].

Industrial standards, both ISO[iii] and API[iv], provide a method for estimating the wind speed from measurements taken at different heights and/or time steps.

Knowing the wind speed at height z_r and time step t_0, first the mean wind speed for the same time step t_0 at a different height z is evaluated with the following formula:

$$U(z) = U(z_r)\left(1 + 0.0573\sqrt{1 + 0.15U(z_r)}\ln\left(\frac{z}{z_r}\right)\right)$$

Then the wind speed corresponding to an average wind period $t \leq t_0$ is given by:

$$U(z,t) = U(z)\left(1 - 0.41I_n(z)\ln\left(\frac{t}{t_0}\right)\right)$$

Where I_n is the turbulence intensity at level z given by:

$$I_n(z) = 0.06\left(1 + 0.043U(z_r)\right)\left(\frac{z}{z_r}\right)^{-0.22}$$

Processing

To improve the quality of the results, the evaluation of extreme winds is based on projections with a daily step. The projections used are the daily maximum wind speeds, corrected to the daily maximum wind speeds from the ERA5/ERA5-Land reanalysis. The instantaneous projections of maximum wind speeds are, after correction, homogeneous with hourly wind speeds.

Return levels for a selection of return periods are then computed using extreme value analysis. Extrapolation to finer temporal resolutions is then performed on the previously computed extreme wind return values.

Sea level rise

Data

Sea level projections are from the Intergovernmental Panel on Climate Change's 6th Assessment Report[v] retrieved from NASA's Physical Oceanography Distributed Active Archive Center.

The results are displayed for the valid data point closest to the location of interest.

Medium and low confidence projections

The AR6 features two sets of projections for sea level:

- "Medium confidence" projections include only processes that can be projected skillfully with at least medium confidence,
- "Low confidence" projections consider processes whose quantification is highly uncertain regarding the timing of their possible onset and/or their potential to accelerate sea level rise.

The differences between the two projections lie primarily in the methodology used to assess the contribution of the Antarctic and Greenland ice sheets to sea level rise.

Both projections are usually similar in the short term, but low confidence projections tend to be higher starting from the second half of the 21st century:

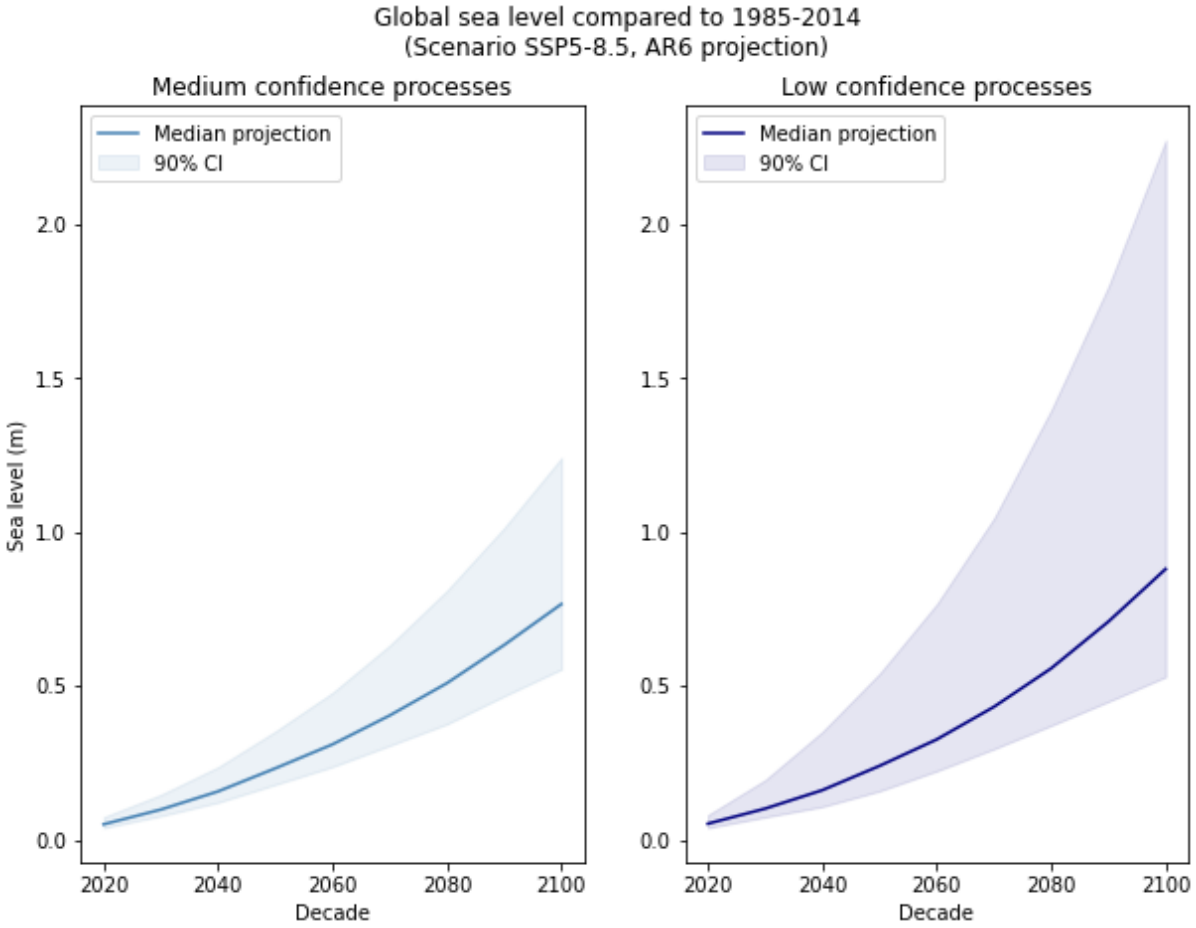

For example, by 2100 in a high emission scenario (SSP5-8.5) the median projection for global sea level rise compared to 1985-2014 level is 0.766 meters in the medium confidence projection and 0.88 m in the low confidence projection.
Uncertainties are also significantly higher: under the same assumptions, the upper bound of the 90% confidence interval is 1.242 m in the medium confidence projection but 2.274 m in the low confidence projection.

The most appropriate projection depends on the lifespan of the project, on its ability to adapt to a faster-than-expected sea level rise, and on the level of risk that is deemed acceptable.
According to the IPCC[vi,vii], stakeholders that are risk tolerant (e.g., those planning for investments that can be easily adapted to unforeseen conditions) may prefer to use projections in the medium confidence range while those with a low risk tolerance (e.g., those planning for long-term investment in critical infrastructure) may wish to consider sea level rise that falls within the high-end scenario.

Since both cases can occur, ClimateVision provides projections from the two sets.

Processing

The original dataset contains sea level projections relative to 1985-2014 level on a 1x1 degree global grid and on 1016 tide gauge locations.

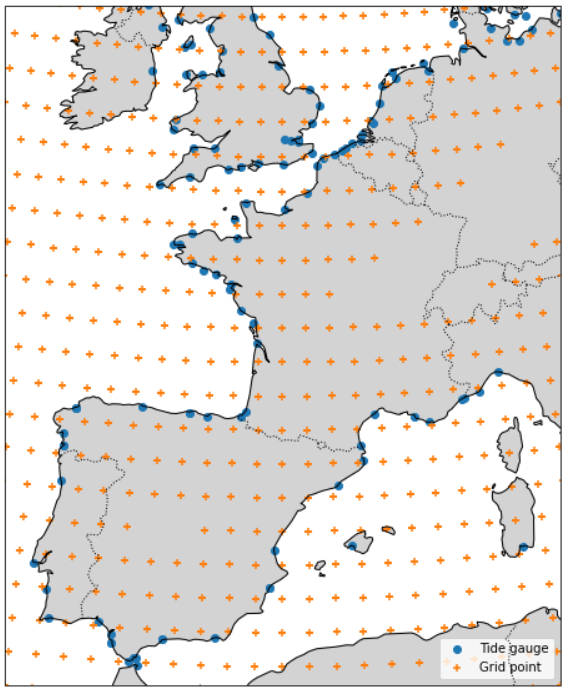

Figure 1: Data points available for west Europe

The results reported correspond to the closest data point to the location of interest.

To remain consistent with the other indicators in the report, the median projection and 90% confidence interval are presented between 2020 and 2080.

Extreme wind wave height

While they evolve with climate change, waves are not among the variables simulated by global circulation models. They are not included in the variables reported in the CMIP5 and 6 projects. The study of the wave evolution in the future typically requires an additional simulation stage to compute heights, periods and directions from climate model outputs, such as wind projections.

However, some wave projections are available from several sources, for example: COWCLIP[1], CSIRO[2] or Copernicus[3]. These projections have been used in many studies to quantify the impact of climate change on sea state, including studies of extreme waves[viii].

[1] https://catalogue.aodn.org.au/geonetwork/srv/eng/catalog.search#/metadata/1de0e8b1-4777-4526-b3d7-805938b8e6bc?uuid=1de0e8b1-4777-4526-b3d7-805938b8e6bc
[2] https://data.csiro.au/collection/csiro:13500v2
[3] https://cds.climate.copernicus.eu/cdsapp#!/dataset/sis-ocean-wave-timeseries

Such publications regularly highlight significant uncertainties[ix], often greater than the projected evolution[x].

Wave projections using the new climate models and emission scenarios from the 6th IPCC report are less common and do not yet seem to have been consolidated at the international level.

Data

ClimateVision provides local waves data extracted from the first CMIP6 projections available and acquired directly through their producers:

- The Australian CSIRO[xi] recently published global wind-wave projections[4] for a small subset of 2 scenarios (SSP1-2.6 and SSP5-85) and 8 models. The spatial resolution of this set of projections is 0.5° with a 3-hour time step. Projections are available for only one value of the wind-drag coefficient (CDFAC): 1[5]. The projections used in this report are based on a coefficient of 1.

A frequent review of publications is carried out to progressively integrate other projections based on the CMIP6 models and scenarios once they are published.

Extreme waves projections are based on WAVEWATCH III simulations forced by future climate from 8 climate models of the Coupled Model Intercomparison Project phase 6, retrieved from the Australian CSIRO. These significant wave height projections use a 3-hour time step that are aggregated into daily maximum significant wave height series.

The SPP2-4.5 scenario is not available. Only the 2071 to 2100 period is available for the projections. The valid data point closest to the location of interest is extracted.

INDICATOR	PROJECTION	REFERENCE
SIGNIFICANT WAVE HEIGHT	CMIP6 hs (daily significant wave height maximum computed from 3-hourly hs)	ERA5 swh (daily significant wave height maximum computed from hourly swh *significant height of combined wind waves and swell*)

Methodologies

[4] https://data.csiro.au/collection/csiro:53176
[5] The wind-drag coefficient is a dimensionless value quantifying the aerodynamic friction between air and sea.

Significant wave height

The significant wave height (H_s) is a statistical measure of the height of waves during a given period. It was originally defined as the average height of the highest one-third of waves. Currently, significant wave height is often taken as 4 times the standard deviation of the water surface elevation series, typically over a period of approximately 30 min[xii,xiii].

The maximum wave height (H_{max}) is the maximum height of an individual wave for a given return period.

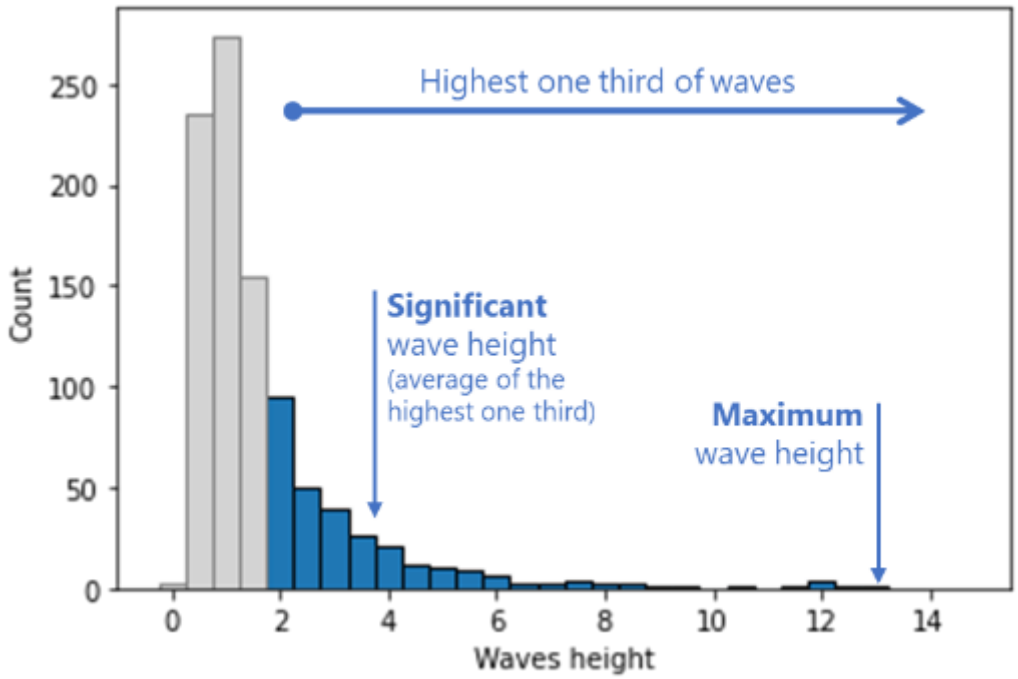

Figure 2: Significant and maximum wave height for a sample of 1000 waves generated using the Pierson-Moskowitz spectrum

The wave period can be evaluated in different ways. The most common definitions are:

- Spectrum peak period (T_p): the period corresponding to the peak of the spectrum[xiv],
- Mean wave period (T_{m01}): the wave period corresponding to the mean frequency of the spectrum[xv],
- Mean zero crossing wave period (T_{m02}): the time obtained by dividing the record length by the number of down crossings (or up crossings) in the record[xvi,xvii],

Other existing definitions include the significant wave period (approximately equal to the spectrum peak period) and the wave energy period (corresponding to the weighted average of the wave energy).

Wave characteristics are largely dependent on atmospheric parameters and evolve with climate change. For example, the IPCC's AR6 reports an increase in wave heights of order

0.5 cm per year, most pronounced in the Southern Ocean. But this trend is affected by significant uncertainties and rated only "medium confidence"[xviii].

Evaluation of the maximum wave height

In addition to the significant wave height derived from models' outputs, the maximum wave height is evaluated using the Rayleigh distribution[xix]. Assuming that the elevation of sea surface has a gaussian distribution, the maximum values of the elevation (i.e.: the maximum wave height) should follow a Rayleigh distribution. In that case the probability that waves reach a height H is:

$$Q(H) = e^{-2\left(\frac{H}{H_s}\right)^2}$$

Where H_s is the significant wave height. As a result, the wave height associated with the probability Q is:

$$H = H_s\sqrt{-\frac{1}{2}\ln Q}$$

For instance, the value of the last centile of wave height is:

$$H = H_s\sqrt{-\frac{1}{2}\ln(0.01)} \approx 1.52H_s$$

A simplified version of this formula is frequently used for off-shore structure calculation:

$$H = 1.86H_s$$

This formula matches to the Rayleigh distribution with an exceedance probability of 0.1%.

Evaluation of the spectrum peak period associated with extreme wave height

As the extremes of significant wave heights are calculated from a statistical model, waves of this height do not necessarily exist in observations or projections. As a result, the period associated with these extremes must be estimated theoretically. The wave period associated with significant wave height extremes is calculated using the following formula:

$$T_p = a + b\sqrt{H_s}$$

Where H_s is the significant wave height and coefficients a and b are adjusted using the observed extremes. However, the fit can sometimes be considered inconclusive with a low the coefficient of determination (R^2 close to 0). In such cases, the approach based on

Goda's formula [xx] has been used to calculate the peak wave period, but shows no improvement compared to a poor fit on the local data.

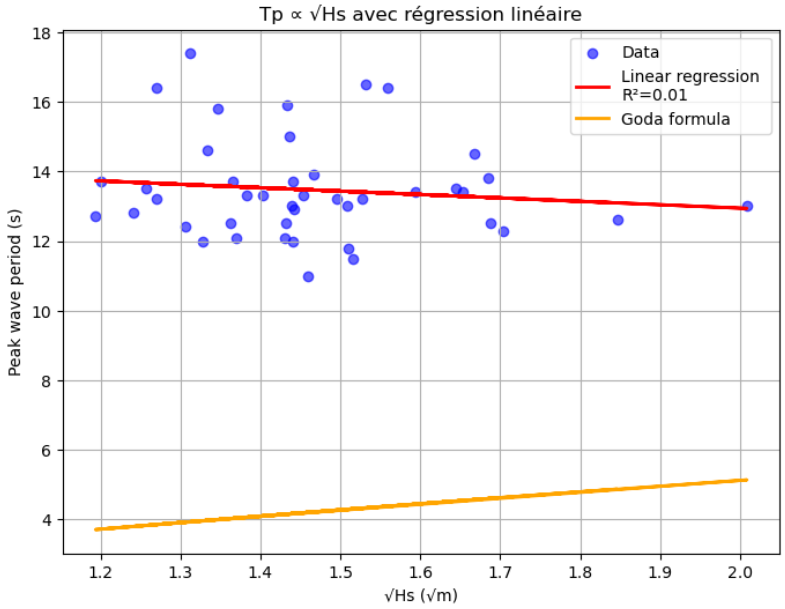

Figure 3 : Peak wave period expressed with the square root of yearly maximum significant wave height. In red the adjusted formula with a poor fit, and in orang the Goda formula.

A more detailed investigation will be conducted in future versions.

Processing

ClimateVision provides an estimate the local evolution of wind waves with climate change, including their period, the significant wave height and the maximum wave height.

Following aggregation into daily maximum series, significant wave height projections are bias-corrected using the CDF-t method. Return levels for a selection of return periods are then computed using extreme value analysis.

Maximum wave heights are computed using the Rayleigh distribution. Finally, the associated peak wave periods are derived from the fit performed on the reference data.

Overview of secondary indicators

This section presents the methodologies used to compute so-called secondary indicators. These indicators are derived from one or more bias-corrected projection time series.

Methodology for wind energy yields

Wind yield model

The wind yield model used in this project is based on two key elements: the wind turbine power curve and equivalent wind speed.

Wind turbine power curve

The wind turbine power curve explicit how a turbine responds to varying wind speeds. The power curve is specific to each wind turbine model. Its description in tabular form (or choice among predefined models) will be one of the main inputs of the tool.

Windspeed[m/s]	Power[kW]
3.0	46
3.5	164
4.0	325
4.5	523
5.0	765
5.5	1052
6.0	1392
6.5	1787
7.0	2245
7.5	2767
8.0	3357
8.5	4006

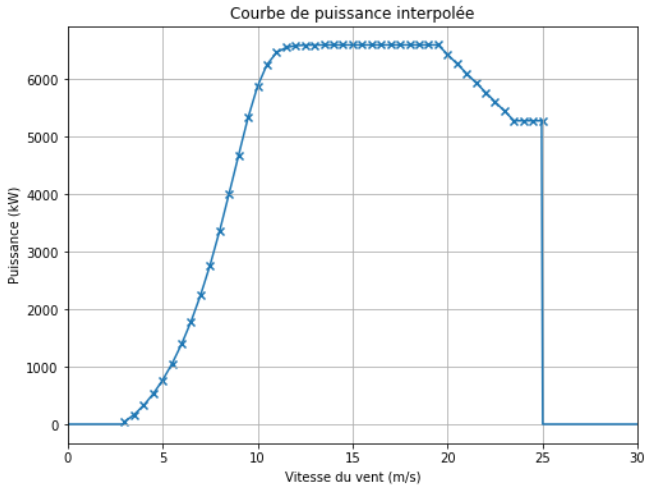

Figure 4 : Wind power curve example, tabular data (left) and interpolated curve

The power curve allows to evaluate the energy production from wind speed with the following formula:

$$E = \sum_{n} P\big(v(n)\big) \times step$$

With:

- $\boldsymbol{E}$: energy production (MWh)
- $\boldsymbol{P(v)}$: power as a function of wind speed (MW)
- $\boldsymbol{v(n)}$: average wind speed over time step n ($m.s^{-1}$)
- $\boldsymbol{step}$: wind sample time step (hours)

Equivalent wind speed

Wind turbines generate power based on the kinetic energy of the wind. Kinetic energy of the wind depends on wind speed but also on air density, which is affected by temperature: as temperature increases, air density decreases, and vice versa.

Equivalent wind speed is used to provide a more accurate representation of the effective wind speed for power generation by considering the impact of temperature on air density. Equivalent wind speed is calculated as:

$$v_{eq}(n) = \left(\frac{T_0}{T(n)}\right)^{1/3} v(n)$$

With:

- $\boldsymbol{v_{eq}(n)}$: equivalent wind speed (actual wind speed adjusted to account for the effect of temperature on air density) over time step $\boldsymbol{n}$
- $\boldsymbol{T(n)}$: average air temperature over time step $\boldsymbol{n}$ (K)
- $\boldsymbol{T_0}$: reference temperature (288.15K)
- $\boldsymbol{v(n)}$: average wind speed over time step $\boldsymbol{n}$ ($m.s^{-1}$)

Therefore, the complete model can be written as:

$$E = \sum_n P\left(\left(\frac{T_0}{T(n)}\right)^{1/3} v(n)\right) \times step$$

With:

- $\boldsymbol{E}$: energy production (MWh)
- $\boldsymbol{P(v)}$: power as a function of wind speed (MW)
- $\boldsymbol{step}$: wind sample time step (hours)
- $\boldsymbol{T(n)}$: average air temperature over time step n (K)
- $\boldsymbol{T_0}$: reference temperature (288.15K)
- $\boldsymbol{v(n)}$: average wind speed over time step n ($m.s^{-1}$)

Model validation

To assess the reliability and accuracy of this wind yield model, validation against real-world data was conducted. Real data are based on wind, temperature and production measured from three turbines in the same farm during two years.

The modelized production was calculated from actual wind speed and temperature using the model described above. It was then compared to actual production corrected to account for down times.

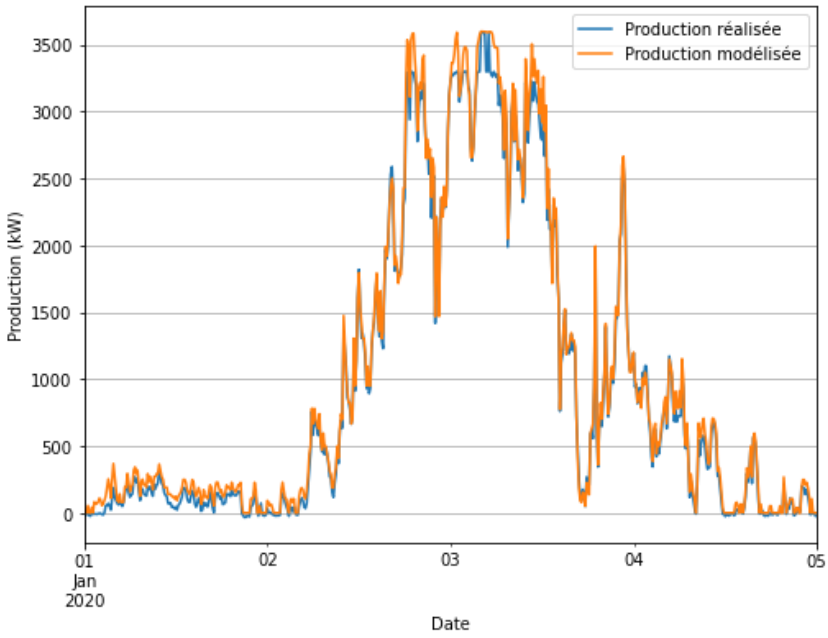

Figure 5 : Comparison between modelized (orange) and actual (blue) productions on a subset of the data

The comparison between the model-predicted production and actual data reveals a mean absolute error (MAE) between 5% and 7% and a coefficient of determination (r^2) above 0.99.

Turbine	MAE	r^2
E1	5,8 %	0,994
E2	7,0 %	0,991
E3	5,3 %	0,995

The MAE gauges the average magnitude of the discrepancies between the predicted and observed values, indicating a good level of precision in wind yield estimations. The coefficient of determination indicates very high correlation between predicted and actual outcomes.

A more detailed examination of errors reveals that the bias is on average positive, meaning that the model tends to slightly overestimate the production. Notably, this bias remains consistent and is not influenced by temperature variations, wind speed fluctuations, or production quantiles. This stability in bias suggests that the model maintains its accuracy across diverse environmental conditions and energy production levels.

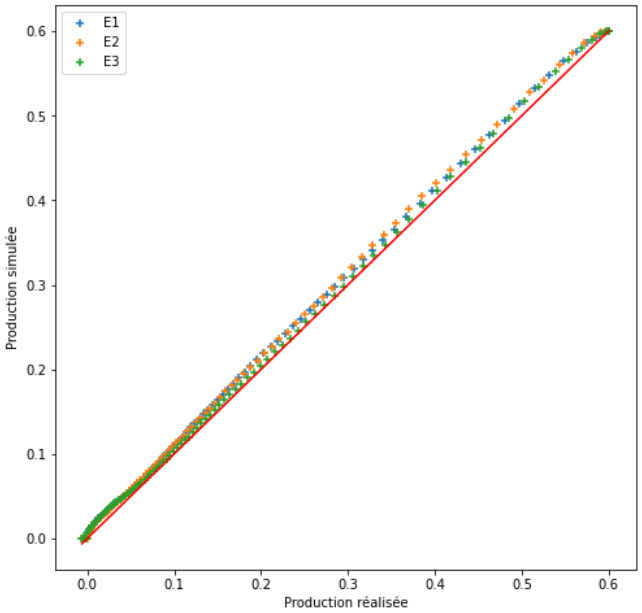

Figure 6 : Quantile-quantile comparison between modelized and actual production

Assessment of model sensitivity to temporal resolution

The previous evaluation was performed using data with a 10-minute time step. However, real-world climate data usually have coarser temporal resolutions, such as hourly, daily or monthly averages. In particular, climate projections are not available with a granularity below 3-hours, as a result it is important to investigate the sensitivity of the wind yield model to different time steps.

To achieve this, we resampled the original fine-grained wind and temperature data at different time steps: 1, 3, 6, and 24 hours, as well as monthly averages, mirroring the temporal resolutions encountered in actual climate reanalysis and climate projections. Then we calculated the modelized production from those upscaled data and compared it to actual production.

Method	**E1**	**E2**	**E3**
Actual production	30625.6	28494.3	29740.7
Modelized (original data, step = 10 minutes)	32198.4	30127,5	30662,9
Modelized (upsampled, step = 1h)	32099.7	29980.0	30541.4
Modelized (upsampled, step = 3h)	31919.7	29767.3	30349.9
Modelized (upsampled, step = 6h)	31721.4	29555.0	30147.4
Modelized (upsampled, daily)	31049.2	28765.3	29448.9
Modelized (upsampled, monthly)	26980.1	24393.4	25380.8

Notably, larger time steps did not result in a discernible degradation of the model's accuracy in assessing average production. This result suggests that the wind yield model maintains its reliability even when exposed to coarser temporal resolutions, making it adaptable to a range of data scenarios.

However, when confronted with monthly average data, high biases were observed for both upper and lower production quantiles. As a result, the model may struggle to generalize effectively with such a low temporal resolution and using monthly data might lead to inaccuracies in capturing extreme production values.

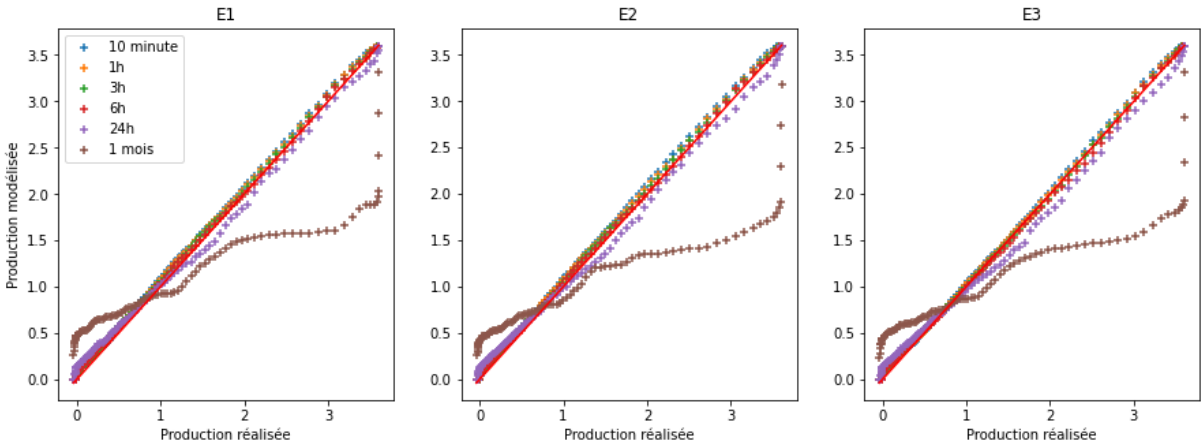

Figure 7 : Quantile-quantile comparison between modelized and actual production for different time steps

In contrast, the model showed no or limited degradation in quantile-quantile dispersion with intermediate time steps (1, 3, 6, and 24 hours). This suggests that the wind yield model can accommodate these time intervals without compromising its predictive accuracy.

Wind height correction

In both reanalysis and climate projections, the wind speed is given at 10 meters. Wind turbines are much higher, usually between 60 and 120 meters, and as a result exposed to stronger winds. A conversion is therefore performed using a logarithmic wind profile:

$$V(h) = V(10) \times \frac{\ln\left(\frac{h}{z_0}\right)}{\ln\left(\frac{10}{z_0}\right)}$$

Where:

- $\boldsymbol{h}$ is the turbine height,
- $\boldsymbol{V(10)}$ and $\boldsymbol{V(h)}$ is the wind speed at 10 meters and at the turbine height respectively
- $\boldsymbol{z_0}$ is the roughness length

The roughness length is a measure of the height and density of obstacles on the ground. The higher it is, the faster wind speed decreases in proximity of the surface.

The following table gives the order of magnitude of the roughness length for different types of environments[xxi]:

Terrain type	Typical roughness length (m)
Very flat terrain (snow, desert)	0.001 - 0.005
Open terrain (grassland, few trees)	0.01 - 0.05
Suburban terrain (buildings 3–5 m)	0.1 - 0.5
Dense urban (buildings 10–30 m)	1 - 5

In the cases considered here, the ground is likely to be open, so the roughness length should be between 0.01 and 0.05 meters. The value initially chosen is 0.01, but this can be adjusted.

Processing

Wind power production is computed from bias-corrected projections of daily wind speed (sfcWind) and daily air temperature (tas). The R2D2 method is employed to restore inter-variable consistency in these climate projections, which have previously been bias-corrected using the CDF-t approach.

Methodology for PV energy yields

Photovoltaic technologies

The most widely used photovoltaic technologies include crystalline silicon cells (cSi), cadmium telluride (CdTe) photovoltaics, and copper indium gallium selenide (CIS) solar cells.

The PV yield model introduced below enables the consideration of these different photovoltaic technologies

PV yield model

The solar PV yield model used in this project is the Huld model[xxii]. Une mise à jour (Anatoli Chatzipanagi, 2025) de ce modèle pour permettre la prise en compte de différentes technologies de cellules photovoltaiques a été réalisée début 2025. Cette dernière est présentée ici.

This model evaluates the production from temperature and irradiance as:

$$P(G',\,T') = P_{peak} \times G' \times \begin{pmatrix} 1 + k_1 \ln(G') + k_2 \ln(G')^2 \\ +T' \times (k_3 + k_4 \ln(G') + k_5 \ln(G')^2) \\ +k_6 T'^2 \end{pmatrix}$$

Where:

- G' is the normalized irradiance:

$$G' = \frac{G}{G_{ref}}$$

- T' is the normalized surface temperature of the modules:

$$T' = T + \frac{G}{u_0 + u_1 . V}$$

With:

- $\boldsymbol{T}$: the air temperature (K)
- $\boldsymbol{G}$: the irradiance (W.m^{-2})
- $\boldsymbol{P_{peak}}$: the installation peak power (MW$_{peak}$)
- $\boldsymbol{G_{ref}}$: the reference irradiance s (1000 W.m^{-2})
- $\boldsymbol{V}$: the wind speed (m.s^{-1})
- $\boldsymbol{u_0}$,$\boldsymbol{u_1}$: coefficients u_0 and u_1 for the cSi, CdTe and CIS modules

Technology	$\boldsymbol{u_0}$ W/(°C.m²)	$\boldsymbol{u_1}$ W.s/(°C.m³)
cSi	26.91	6.20
CdTe	23.37	5.44
CIS	22.64	3.60

- $\mathbf{k_1}$, $\mathbf{k_2}$, $\mathbf{k_3}$, $\mathbf{k_4}$, $\mathbf{k_5}$, $\mathbf{k_6}$: the parameters of the model (module type-dependent)

k parameters (or the selection between a set of predefined parameters) will be one of the inputs of the tool.

Coefficients	**cSi**		**CdTe**		**CIS**	
	Original	**Updated (2025)**	**Original**	**Updated (2025)**	**Original**	**Updated (2025)**
k_1	−0.017237	−0.006756	−0.046689	−0.020644	−0.005554	−0.011001
k_2	−0.040465	−0.016444	−0.072844	−0.035136	−0.038724	−0.029734
k_3	−0.004702	−0.003015	−0.002262	−0.003406	−0.003723	−0.002887
k_4	0.000149	−0.000045	0.000276	0.000073	−0.000905	0.000217
k_5	0.000170	−0.000043	0.000159	−0.000141	−0.001256	−0.000163

k_6	0.000005	0.000000	−0.000006	0.000002	0.000001	0.000000

Model validation

To assess the reliability and accuracy of our PV yield model, validation against real-world data was conducted.

Real data are based on irradiance, temperature and production measured from a solar farm between 1994 and 2022. The modelized production was calculated from actual irradiance and temperature using the model described above. It was then compared to real-world production corrected to account for downtimes and modules orientation.

The comparison between the model-predicted production and actual data reveals a mean absolute error (MAE) of approximately 4% and a coefficient of determination (r^2) above 0.995.

Period	**MAE**	**r^2**
1994-2003	3,8 %	0,998
2004-2013	3,8 %	0,998
2014-2022	3,9 %	0,998

The MAE gauges the average magnitude of the discrepancies between the predicted and observed values, indicating a very good level of precision in yield estimations. The coefficient of determination indicates near-perfect correlation between predicted and actual outcomes.

A more detailed examination of errors reveals that the bias is on average slightly negative, meaning that the model tends to underestimate the production.

Notably, this bias remains consistent and is not influenced by irradiance, temperature or production quantiles. This stability in bias suggests that the model can generalize properly as it maintains its accuracy across diverse environmental conditions and energy production levels.

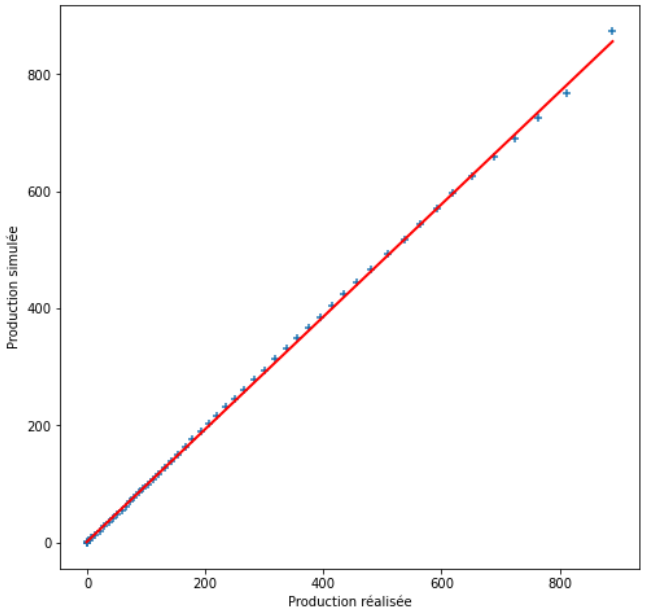

Figure 8 : Quantile-quantile comparison between modelized and actual production

Assessment of model sensitivity to temporal resolution

The model validation was performed using data with a 1-hour time step. Real-world climate data often exists at coarser temporal resolutions. Climate projections are not available with a granularity below 3-hours, as a result it is important to investigate the sensitivity of the PV yield model to different time steps.

To achieve this, we resampled the original irradiance and temperature data at different time steps: 3, 6, and 24 hours, as well as monthly averages, mirroring the temporal resolutions encountered in actual climate projections. Then we calculated the modelized production from those upscaled data and compared it to actual production.

Method	**Production**
Actual production	35781.5
Modelized (original data, step = step = 1h)	34772.0
Modelized (upsampled, step = 3h)	34740.9
Modelized (upsampled, step = 6h)	34931.1
Modelized (upsampled, daily)	34612.6
Modelized (upsampled, monthly)	34642.3

Larger time steps did not result in a degradation of the model's accuracy for average production. This suggests that the PV yield model maintains its reliability even when exposed to coarser temporal resolutions, making it adaptable to a range of data scenarios.

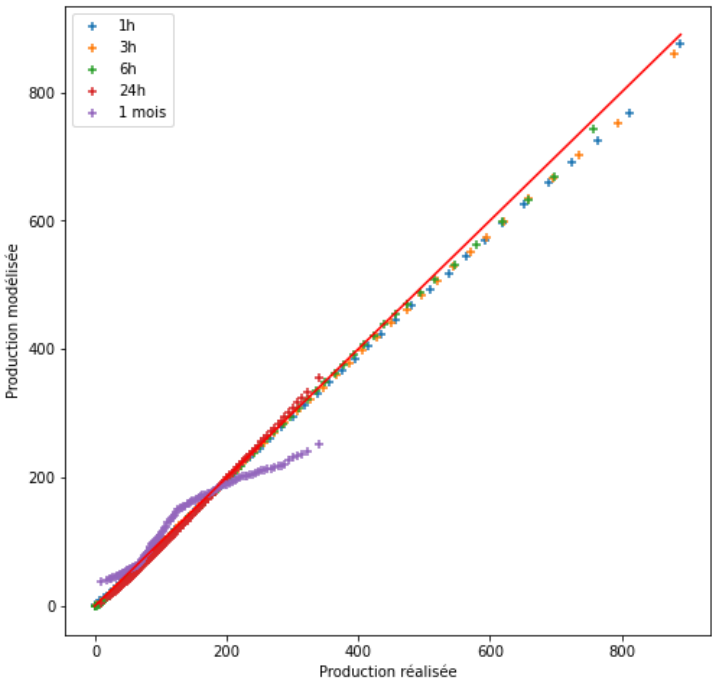

Figure 9 : Quantile-quantile comparison between modelized and actual production for different time steps

However, when confronted with monthly averaged data, high discrepancies were observed in the quantiles' distribution, especially for upper production quantiles. As a result, monthly climate data might lead to inaccuracies in capturing PV yield especially during high-production periods.

In contrast, the model showed no significant degradation in results with intermediate time steps (3, 6, and 24 hours). This suggests that the solar yield model can accommodate these time intervals without compromising its predictive accuracy.

Processing

Solar power production is computed from bias-corrected projections of daily solar irradiance (rsds), daily air temperature (tas) and daily windspeed (sfcWind). The R2D2 method is employed to restore inter-variable consistency in these climate projections, which have previously been bias-corrected using the CDF-t approach.

Climate models

Climate models, also known as general circulation models or GCMs, use mathematical equations to characterize how energy and matter interact in different parts of the ocean, atmosphere, land.

Approximately 100 global circulations models participate in the Coupled Model Intercomparison Project phase 6 (CMIP6). To limit the resources required for the studies,

especially in terms of time needed for data access and computing power, ClimateVision uses a subset of models.

Models for atmospheric indicators

To ensure consistency and comparability, the same climate models are used for all atmospheric indicators. In ClimateVision V1.1.0, these indicators include mean temperature, maximum temperature, minimum temperature, mean precipitation, maximum precipitation, maximum wind speed, sea level rise, and maximum significant wave height.

Models were selected based on 3 criteria:

- Data availability
- Equilibrium climate sensitivity
- Model independence

Due to the recent publication of model data, studies on their regional performance are still scarce and usually only consider a subset of the models currently available. As a result, this criterion was not considered in ClimateVision V1.1.0 but will be added in later versions.

Data availability

The models were selected primarily based on data availability, as some projections are unavailable. Climate models were prioritized based on the range of climate parameters they provide. To maximize the number of models available, only three emissions scenarios are considered in the current version:

- SSP1-2.6: low emission scenario, representative of an emission trajectory that keeps global warming below 2°C
- SSP2-4.5: intermediate emissions scenario, close to current emission trajectory
- SSP5-8.5: very high emissions scenario that can be used as a worst case

Other scenarios not included are: SSP1-1.9, SSP3-7.0 and SSP4-6.0. Both SSP1-1.9 and SSP4-6.0 are “tier 2” (or low priority) SSP[xxiii]. And SSP3-7.0 is a high emissions scenario intermediary between SSP2-4.5 et SSP5-8.5.

Equilibrium climate sensitivity

Equilibrium climate sensitivity (ECS) is the long-term warming that would occur if the concentration of CO_2 in the atmosphere were to double. According to the IPCC 6th Assessment Report the best estimate for equilibrium climate sensitivity is 3°C with a likely range of 2.5 to 4°C and a very likely range of 2 to 5°C.[xxiv]

Several GCMs of CMIP6 have ECS that fall outside this range either below (low-likelihood, low warming) or above (low-likelihood, high warming). Because one of those models can significantly alter the results on a small ensemble, an increasingly common practice in the scientific literature is to downweigh models with ECS values outside the assessed range or simply exclude them from ensembles[xxv,xxvi].

In practice, this criterion leads to the exclusion of the Russian model (INM-CM5-0) from our list of candidates[xxvii]. The latter is left on the list and is used until new models are added. It will be removed shortly.

Model's independence

Even when they are exploited by different institutions, climate models are not necessarily independent of each other: they can use similar assumptions or common modules. The use of several closely related models in an ensemble could therefore result in an overweighting of the corresponding trajectory.

The studies on the correlations between models are still significantly less complete than for the CMIP5 generation[xxviii]. One publication investigating 33 CMIP6 model suggests the following dependency tree[xxix]:

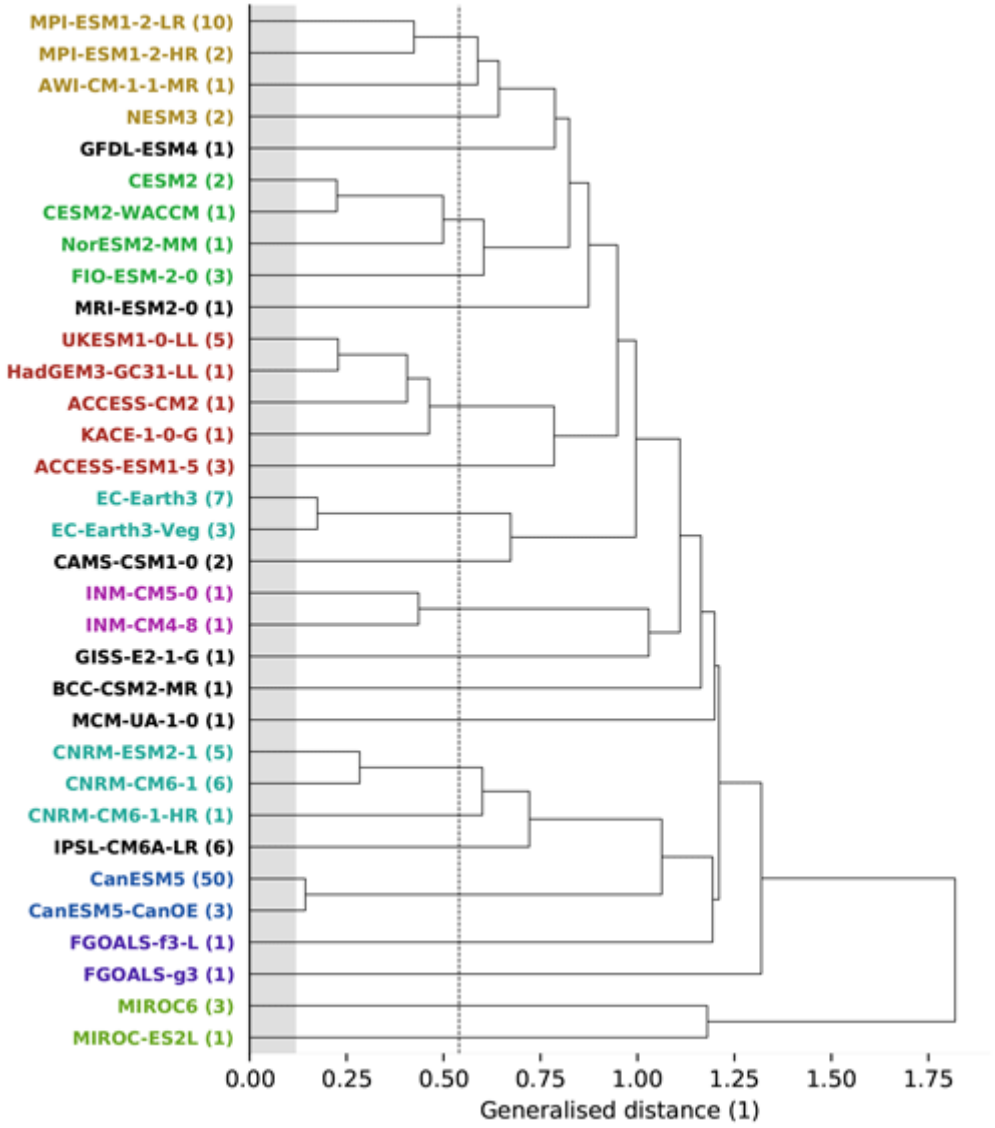

Models branching further to the left are more dependent, and models branching further to the right are more independent. An estimate of climate natural variability is indicated using gray shading, models that have a distance similar to this value (for instance CanESM5 and CanESM5-CanOE) are statistically indistinguishable. Models branching after the dotted line are reasonably independent.

Models set

The ideal models' ensemble should meet the following conditions:

1. It includes enough models (at least 10),
2. It provides projections for all desired variables,
3. It provides projections for all scenarios,
4. It does not include models with ECS outside the IPCC's very likely range,
5. It prioritizes models that perform well on the study area, and ideally on the whole planet,

6. If possible with respect to the previous conditions, it does not include closely related models.

The ensemble of models that best fit these objectives is the following:

Model	ripf
AWI-CM-1-1-MR*	r1i1p1f1
FGOALS-g3*	r1i1p1f1
CanESM5	r1i1p2f1
CMCC-ESM2	r1i1p1f1
CNRM-CM6-1	r1i1p1f2
CNRM-ESM2-1	r1i1p1f2
ACCESS-ESM1-5	r5i1p1f1
EC-Earth3*	r4i1p1f1
INM-CM5-0	r1i1p1f1
IPSL-CM6A-LR	r2i1p1f1
MIROC6	r2i1p1f1
MIROC-ES2L	r1i1p1f2
UKESM1-0-LL	r4i1p1f2
MPI-ESM1-2-LR	r5i1p1f1
MRI-ESM2-0	r1i1p1f1

*not used in V1.1.0 but available

Statistical downscaling

Methodology

Global and regional climate models' resolution is often lower than desired and they are in general biased. As a result, bias correction and downscaling are widely used in climate impact modelling.

Bias correction is the process of adjusting climate model outputs to account for their systematic errors. Numerous statistical bias correction methods exist. The essence of these methods is to build a transformation that fits the simulations on a past reference period to the observations on this same period, then apply the same transformation to future climate simulations with the fundamental assumption that it will remain valid in the future.

No method can be considered as entirely reliable[xxx], the choice of a suitable method depends on the use case but also on the needs and technical constraints of each project (e. g.: explicability, computational efficiency…).

At this stage, ClimateVision employs one method: the Cumulative Distribution Function transform (CDF-t) for all the variables.

The CDF-t method[xxxi], a well-established variation of the quantile-quantile method. It effectively corrects biases while preserving trends in future scenarios. It has been used in numerous research and adaptation projects.

CDF-t principle

The CDF-transformation method shares the same philosophy of quantile-quantile bias correction methods. CDF-t differs from typical quantile-quantile methods by considering the change in the large-scale CDFs between the training and the future period. These transfer functions between past and future CDFs correspond to a change in the distribution of the variable of interest over time. The CDF-t method assumes that the evolution over time of the distribution of the global scale variable is identical to the evolution of this local scale variable.

Let V be the number of variables and N be the number of time steps. X_{M_p} is the VxN matrix containing projections. $X_{M_p}^{d}(n)$ is the value of the model simulation for the variable d and the nth time step of the projection period.
Similarly, X_{M_c} and X_{R_c} are the matrixes containing the model simulation and observation records, respectively, for the calibration period.

Let $F^d_{M_p}$, $F^d_{M_c}$ and $F^d_{R_c}$ be the univariate cumulative distribution functions of the model projections, model calibration and records calibration data for the variable d. These distributions can be estimated from the data.

The objective is to calculate $F^d_{R_p}$, the cumulative distribution of observations in the future.

	Calibration (Past reference period)	Projection (Future period)
Model (Simulated weather)	$F^d_{M_c}$	$F^d_{M_p}$
Records (Actual weather)	$F^d_{R_c}$	$F^d_{R_p}$?

Let T be the transfer function between the cumulative distribution function of the observations and projections during the reference period. For any quantile q:

$$F^d_{R_c}(q) = T\left(F^d_{M_c}(q)\right)$$

By inversing this relation, we get:

$$T(u) = F^d_{R_c}\left({F^d_{M_c}}^{-1}(u)\right) \qquad \text{for u in [0, 1]}$$

Assuming time stationarity of the transfer function, the first relation can be applied to the projection period as well:

$$F^d_{R_p}(q) = T\left(F^d_{M_p}(q)\right)$$

By combining the two previous equations, we get:

$$F^d_{R_p}(q) = F^d_{R_c}\left({F^d_{M_c}}^{-1}\left(F^d_{M_p}(q)\right)\right)$$

Once $F^d_{R_p}$ has been estimated, a simple quantile-quantile method is performed to calculate the bias corrected series $\widehat{X^d_{M_p}}$, i.e.:

$$\widehat{X^d_{M_p}}(n) = {F^d_{R_p}}^{-1}\left(F^d_{M_p}\left(X^d_{M_p}(n)\right)\right)$$

The method is applied on a month-by-month basis to avoid processing seasonal data.

R2D2

ClimateVision employs a multivariate bias correction technique for high-dimensional climate simulations, known as Rank Resampling for Distributions and Dependences (R2D2). The method aims to adjust not only the univariate marginal distributions of climate model outputs but also their multivariate dependence structures across variables and sites, which traditional univariate bias correction methods do not account for. R2D2 operates in a marginal/dependence correction framework:

(1) Each statistical dimension (variable at a location) is first corrected independently using a univariate bias correction method, such as the CDF-t approach in ClimateVision.

(2) A "reference dimension" is selected, and its bias-corrected rank sequence is preserved to drive the multivariate reconstruction. By default, ClimateVision employs the primary variable; for instance, when using R2D2 to correct wind and temperature data for the purpose of computing wind power production, the bias-corrected time series of wind speed serves as the reference.

(3) For each time step of a projection period (e.g., future climate), ranks of the reference dimension are matched to ranks in a historical calibration period to identify analogous reference states.

(4) For each match, the corresponding inter-variable and inter-site rank structures from the reference dataset are imposed by shuffling the corrected values, thereby reproducing the empirical copula of the reference.

(5) The procedure is repeated with each dimension serving as reference to create multiple stochastic corrected outputs.

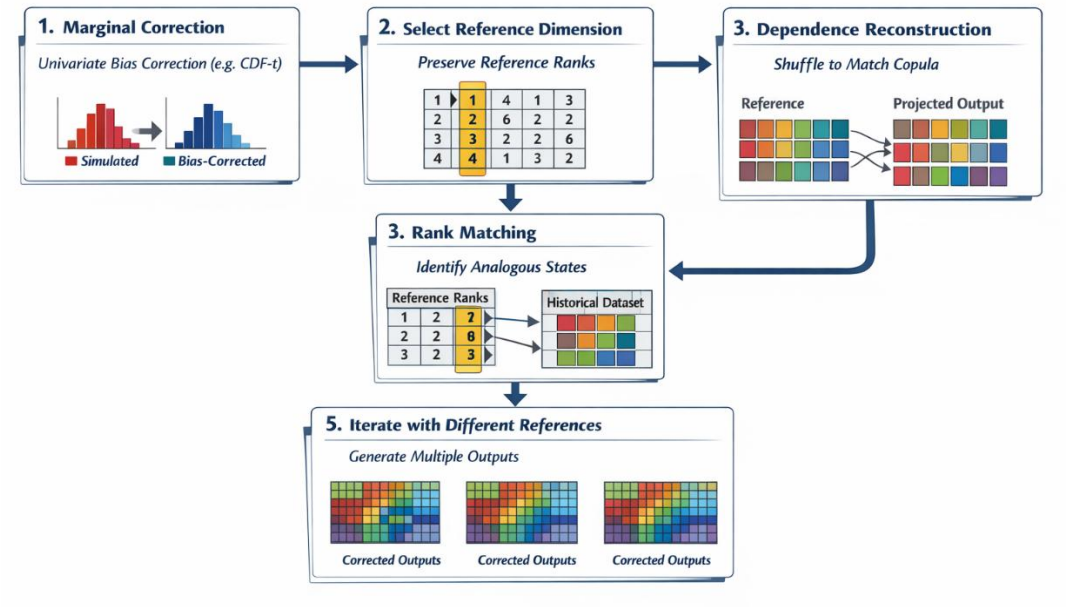

Figure 10: R2D2 workflow

Crucially, R2D2 assumes stationarity of the multivariate dependence (copula) structure over time, enabling its application in high-dimensional contexts (e.g., thousands of grid cells and variables). The approach relaxes the deterministic temporal constraints of

previous copula-based bias correction methods, allowing the climate model to retain its inherent temporal dynamics while preserving inter-site and inter-variable dependencies.

It is important to note that the R2D2 method substantially degrades autocorrelation. Consequently, the resulting data should be used with caution.

Precipitation special case

To correct the precipitation the CDF-t method is combined with the Singularity Stochastic Removal (SSR) approach[xxxii].

Due to the nature of precipitation, additional steps are required for bias correction of this variable. The correction procedure follows these steps:

1. Application of the SSR
2. Transformation using the Log1x function
3. Bias correction using the CDF-t method
4. Transformation using the Exp1x function
5. Application of the inverse SSR

First, a threshold ***th*** is set to 1×10^{-4}mm.day^{-1}. For a time series to be corrected, all values below the threshold ***th*** (including zeros) are replaced by a random value drawn from a uniform distribution over the interval]0 ; ***th*** [. As a result, there are no longer any zero-precipitation values in the dataset. The resulting series is then transformed using the Log1x function.

$$log1x(x) = \begin{cases} x - 1, & if\ x \geq 1 \\ \ln(x), & if\ 0 < x < 1 \\ x, & otherwise \end{cases}$$

The CDF-t bias correction is subsequently applied to this series. After correction, the Exp1x function is applied to the bias-corrected precipitation values.

$$exp1x(x) = \begin{cases} e^x, & if\ x < 0 \\ x + 1, & otherwise \end{cases}$$

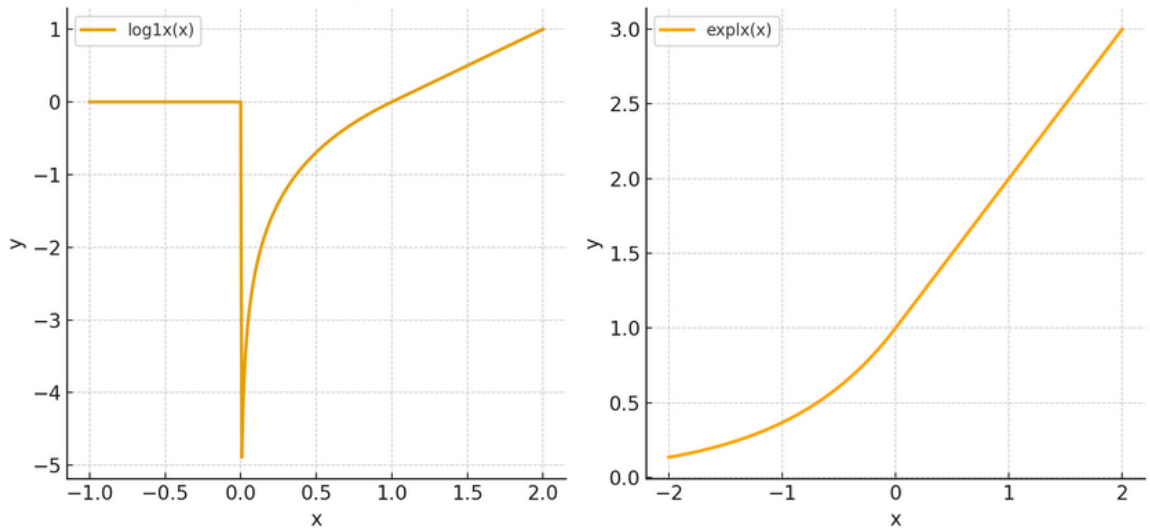

Finally, the inverse SSR is applied by setting values below the threshold ***th*** to zero.

In addition, a security barrier has been implemented for the precipitation extremums. To limit the effects of an overestimation of extreme precipitation, sometimes introduced, by the CDF-t method, an adaptive smoothing approach for the distribution tails was implemented. It is based on the definition of a maximum precipitation threshold **S**, determined as follows:

$$S = \max\{\text{ERA5}\} \times \min\left(1{,}5,\ \frac{Q95(\text{GCM}_{\text{proj}})}{Q95(\text{GCM}_{\text{calib}})}\right)$$

This threshold helps to constrain the excessive amplification of extremes during the projection phase. It depends on the evolution of the 95th percentile of the GCM between the calibration and projection periods, with an upper bound set at +100% relative to observations (ERA5).
In practical terms, for each corrected time series, if the maximum corrected precipitation value **M** obtained from ARRM exceeds this threshold (**M > S**), the upper tail of the distribution is adjusted. The interval **[Q95([GCM$_{\text{proj}}$]), M]** is then reprojected onto **[Q95([GCM$_{\text{proj}}$]), S]**, ensuring a smooth transition while preventing unrealistic extreme values.

Extrapolation of extreme values

Methodological approach and reference

Climatology is generally based on 30-year periods during which the climate is assumed to be stationary. As low probabilities events (typically with a return period of 10 years or more) cannot be computed empirically from 30 years sample they must be extrapolated. Many extrapolation methods are used, and none is universally accepted in the industrial field[xxxiii].

In this project we used a statistical method based on Extreme Value Theory[xxxiv]. The idea of this method is to take extremes values from a weather data sample and fit the tail of the probability distribution with an appropriate extreme value distribution. More specifically, we use the block-maxima approach to select extrema and the maximum likelihood estimation to fit their distribution to a generalized extreme value (GEV) distribution.

This method is similar to the "historical method" recommended in the ISO19901, except that input data are derived from bias-corrected climate projections instead of in-situ measurements or model hindcasts. It is frequently used in climate research[xxxv].

A key advantage of extreme value analysis is that it is highly flexible as it is based on the mathematical proprieties of extreme distribution and not on a knowledge of the underlying physical process. Therefore, the same method can be used to study heatwaves, cold spells, extreme rainfall, etc.
The definition of the blocks is adapted to the variable and location, e.g.: for maximum temperature the block is a calendar year (January-December) in the northern hemisphere and July-June in the southern hemisphere.

Illustration

The extrapolation is based on a sample of 30 years, either from reanalysis for current and past climate or from bias-corrected projections for future climate.

The first step is to select the extreme values from the sample using the block-maxima method: we divide the sample in blocks of similar duration (1 year) and take the highest value in each block:

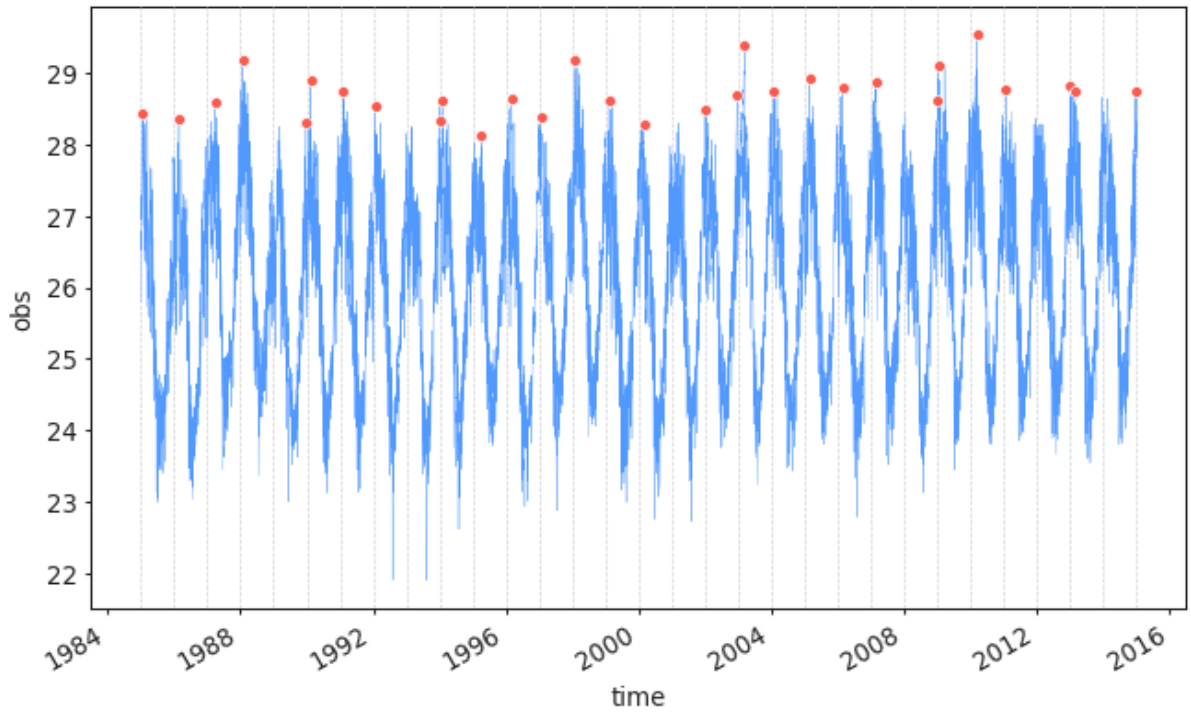

Figure 11: Extreme selection using the block maxima method

Assuming that the selected values are independent and identically distributed, the normalized distribution of block maxima must converge to a generalized extreme value (GEV) distribution:

$$f(x) = \frac{1}{\sigma}\left(1 + \xi\left(\frac{x-\mu}{\sigma}\right)\right)^{-\frac{1}{\xi}-1} e^{-\left(1+\xi\left(\frac{x-\mu}{\sigma}\right)\right)^{-\frac{1}{\xi}}}$$

This mathematical property is known as the Fisher-Tippett theorem. Other distributions can be used, such as the Fréchet, Gumbel or Weibull distributions, but they are in facts special cases of the more general GEV distributions. ClimateVision uses the more general form as it does not require assumptions on the physical properties of the extremes.

The trade-off is that the GEV as three parameters, μ (location), σ (scale) and ξ (shape), while other distributions may have less degree of liberty. This means that fitting our maxima to the GEV (i.e.: choosing value of the parameters that minimize the distance between the empirical and theoretical distributions) will be more complex. Various methods exist and can yield slightly different results, especially for long return periods and/or small samples[xxxvi,xxxvii].

ClimateVision uses maximum likelihood method. The idea is to define the probability to get the observed data as a function of the parameters, then numerically choose the set of parameters that maximize this function. This is a flexible method, widely adopted in

statistics as it can be used to adjust any theorical distribution to observed data, and it usually performs well for extreme value analysis.

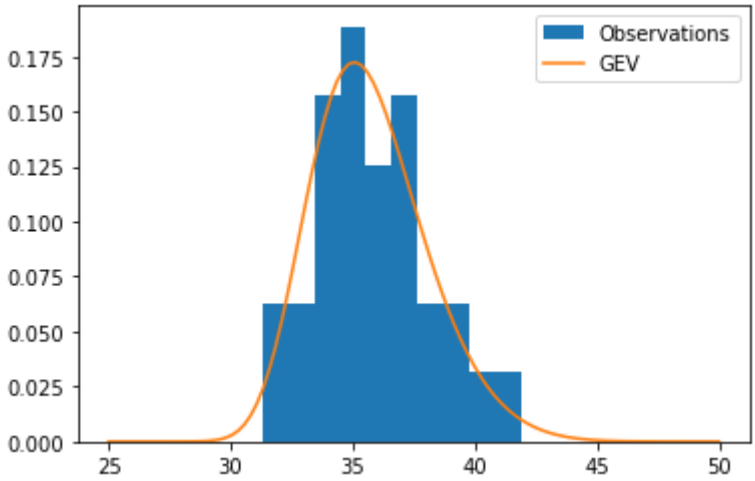

Figure 12: GEV fitted to an empirical distribution of block maxima

The cumulative density function of the fitted GEV can be interpreted as the probability that a value is not exceeded, in other words the long-term frequency of the event "the value x is exceeded" is:

$$\mathrm{f}(x) = P(X \geq x) = 1 - F(x)$$

With:

$$F(x) = \int_{-\infty}^{x} f(u)\, du$$

Conversely, the return period of a given x value is:

$$T(x) = \frac{1}{\mathrm{f}(x)} = \frac{1}{1 - F(x)}$$

This formula and the fitted GEV distribution can be used to estimate the return level associated with any specified return period:

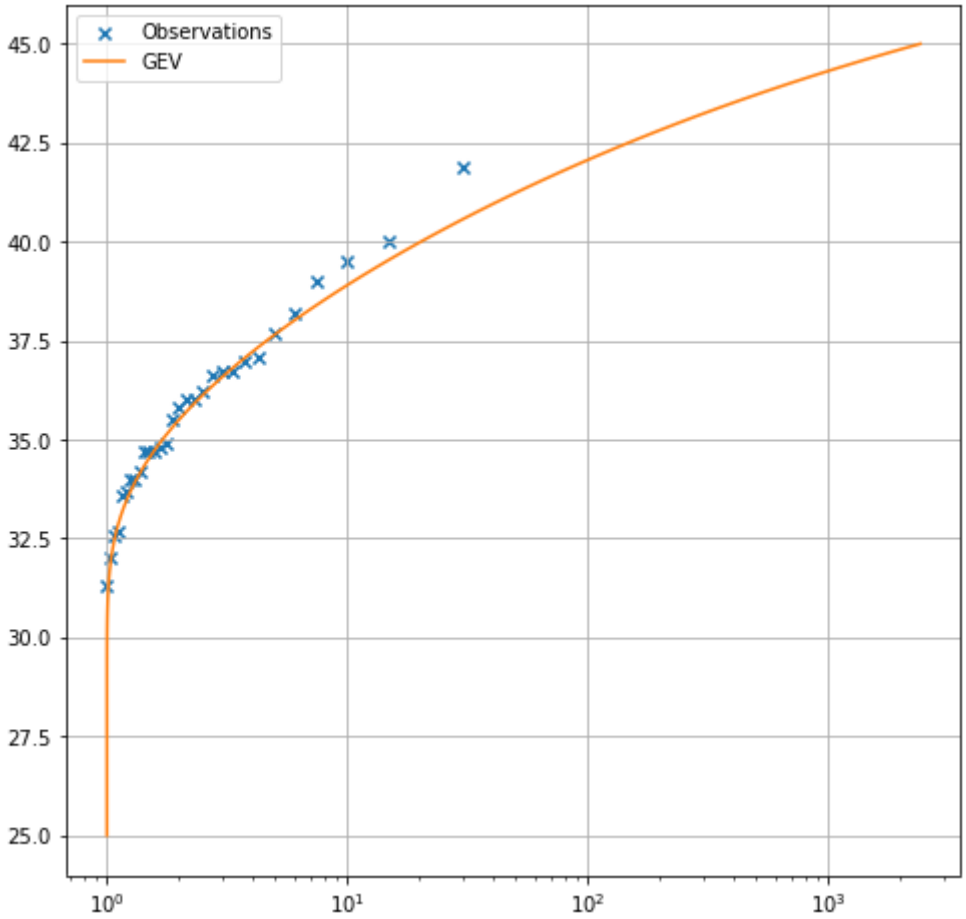

Figure 13: Theoretical and empirical return levels a function of return periods

Minima are computed using the same method simply by inversing the sample data and results:

$$Min(f) = -Max(-f)$$

Appendix A: legal notices

ERA5/ERA5 Land

Contains modified Copernicus Climate Change Service information.

Access to all Copernicus Information and Data is regulated under Regulation (EU) No 1159/2013 of the European Parliament and of the Council of 12 July 2013 on the European Earth monitoring program, under the ECMWF Agreement and under the European Commission's Terms and Conditions. Access to all Copernicus information is regulated under Regulation (EU) No 1159/2013 and under the ECMWF Agreement.
Access to Copernicus Products is given for any purpose in so far as it is lawful, whereas use may include, but is not limited to: reproduction; distribution; communication to the public; adaptation, modification and combination with other data and information; or any combination of the foregoing.
Consult https://cds.climate.copernicus.eu/api/v2/terms/static/licence-to-use-copernicus-products.pdf

CMIP6

CMIP6 model data is licensed under a Creative Commons International License (https://creativecommons.org/licenses/). The exact license may vary depending on the modelling center:

Model	Producer	Country	License
AWI-CM-1-1-MR	Alfred Wegener Institute (AWI)	Germany	CC BY-SA 4.0
FGOALS-g3	Institute of Atmospheric Physics (IAP), Chinese Academy of Sciences	China	CC BY-SA 4.0
CanESM5	Canadian Centre for Climate Modelling and Analysis (CCCma)	Canada	CC BY-SA 4.0
CMCC-ESM2	Centro Euro-Mediterraneo sui Cambiamenti Climatici (CMCC)	Italy	CC BY-SA 4.0
CNRM-CM6-1	Centre National de Recherches Météorologiques (CNRM) & CERFACS	France	CC BY-NC-SA 4.0
CNRM-ESM2-1	CNRM & CERFACS	France	CC BY-NC-SA 4.0
ACCESS-ESM1-5	CSIRO	Australia	CC BY-SA 4.0
EC-Earth3	EC-Earth Consortium	-	CC BY-SA 4.0
INM-CM5-0	Institute of Numerical Mathematics (INM)	Russia	CC BY-SA 4.0
IPSL-CM6A-LR	Institut Pierre-Simon Laplace (IPSL)	France	CC BY-NC-SA 4.0
MIROC6	JAMSTEC, AORI, NIES	Japan	CC BY-SA 4.0
MIROC-ES2L	National Institute for Environmental Studies (NIES)	Japan	CC BY-SA 4.0

UKESM1-0-LL	UK Met Office Hadley Centre & UKESM project partners	United-Kingdom	CC BY-SA 4.0
MPI-ESM1-2-LR	Max Planck Institute for Meteorology (MPI-M)	Germany	CC BY-SA 4.0
MRI-ESM2-0	Meteorological Research Institute (MRI)	Japan	CC BY-SA 4.0

The data producers and data providers make no warranty, either express or implied, including, but not limited to, warranties of merchantability and fitness for a particular purpose. All liabilities arising from the supply of the information (including any liability arising in negligence) are excluded to the fullest extent permitted by law.
Consult https://pcmdi.llnl.gov/CMIP6/TermsOfUse for terms of use governing CMIP6 output, including citation requirements and proper acknowledgment.

CSIRO

CSIRO waves data is licensed under a Creative Commons International License CC BY-SA 4.0 (https://creativecommons.org/licenses/by-sa/4.0/).

Consult https://data.csiro.au/collection/csiro:60106

[i] Kurbatova, M., & al. (2018). *Comparison of seven wind gust parameterizations over the European part of Russia*. Advances in Science and Research. [available online]
[ii] ISO. (2016): Petroleum and natural gas industries — Specific requirements for offshore structures — Part 1: Metocean design and operating considerations (ISO 19901-1:2015), p.20.
[iii] ISO. (2016): *Op. Cit.* p.46.
[iv] American Petroleum Institute. (2014). Recommended practice for planning, designing and constructing fixed offshore platforms. Formula 5.3.
[v] Fox-Kemper, B. & al. (2021). Ocean, Cryosphere and Sea Level Change. In: Climate Change 2021: The Physical Science Basis. Contribution of Working Group I to the Sixth Assessment Report of the Intergovernmental Panel on Climate Change. [available online]
[vi] IPCC. (2019). *IPCC Special Report on the Ocean and Cryosphere in a Changing Climate*. p. 327. [available online]
[vii] Fox-Kemper, B. & al. (2021). *op.cit.* p. 1308.
[viii] Lobeto, H. & al. (2021): *Future behavior of wind wave extremes due to climate change*. Sci Rep 11, 7869. [available online]
[ix] Ewans, K. & al. (2023): *Uncertainties in estimating the effect of climate change on 100-year return value for significant wave height*. Ocean Engineering 272. [available online]
[x] Morim, J. & al. (2023): *Understanding uncertainties in contemporary and future extreme wave events for broad-scale impact and adaptation planning*. Science Advances 9.2. [available online]
[xi] Meucci, A. et al. (2023): 140 years of global ocean wind-wave climate derived from CMIP6 ACCESS-CM2 and EC-Earth3 GCMs: Global trends, regional changes, and future projections. Journal of Climate 36.6: 1605-1631. [available online]
[xii] ISO. (2016): *Op. Cit.* p.7.
[xiii] Martin, P. (2023): How to describe the wave height and wave period parameters? [available online]

[xiv] WMO. (2020): *Guide to wave analysis and forecasting (2018 edition).* p. 19. [available online]
[xv] WMO. (2020): *Op. Cit.* p. 19.
[xvi] WMO. (2020): *Op. Cit.* p. 19.
[xvii] ISO. (2016): *Op. Cit*. p.5.
[xviii] Fox-Kemper, B. & al. (2021): Ocean, Cryosphere and Sea Level Change. In Climate Change 2021: The Physical Science Basis. Contribution of Working Group I to the Sixth Assessment Report of the Intergovernmental Panel on Climate Change. p. 1310. [available online]
[xix] WMO. (2020): *Op. Cit.* p. 14.
[xx] Goda, Y. *Revisiting Wilson's formulas for simplified wind-wave prediction*. J. Waterw. Port Coast. Ocean Eng. 2003, 129, 93–95
[xxi] Holmes, J. (2012). *Wind Loading of Structures*, p.60.
[xxii] Huld, T. & al. (2015): *Estimating PV Module Performance over Large Geographical Regions: The Role of Irradiance, Air Temperature, Wind Speed and Solar Spectrum*. Energies 8, no. 6: 5159-5181. [available online]
[xxiii] O'Neill, B. & al. (2016). *The Scenario Model Intercomparison Project (ScenarioMIP) for CMIP6*. Geosci. Model Dev., 9, 3461–3482. [available online]
[xxiv] Arias, P.A. & al. (2021). Technical Summary. In: Climate Change 2021: The Physical Science Basis. Contribution of Working Group I to the Sixth Assessment Report of the Intergovernmental Panel on Climate Change. [available online]
[xxv] Hausfather, Z. & al. (2022). *Climate simulations: recognize the "hot model" problem*. Nature, 605, 26–29. [available online]
[xxvi] Shiogama, H. & al. (2021). *Selecting CMIP6-based future climate scenarios for impact and adaptation studies.* SOLA. [available online]
[xxvii] Zelinka, M. D. & al. (2020). *Causes of higher climate sensitivity in CMIP6 models*. Geophys. Res. Lett.*,* 47. [available online]
[xxviii] Knutti, R. & al. (2013). *Climate model genealogy: Generation CMIP5 and how we got there*. Geophysical Research Letters, 40(6), 1194-1199. [available online]
[xxix] Brunner, L. & al. (2020). *Reduced global warming from CMIP6 projections when weighting models by performance and independence.* Earth Syst. Dynam., 11, 995–1012, 2020. [available online]
[xxx] Maraun, D. (2016). *Bias correcting climate change simulations-a critical review*. Current Climate Change Reports, 2(4), 211-220. [available online]
[xxxi] Michelangeli, P. A. & al. (2009). *Probabilistic downscaling approaches: Application to wind cumulative distribution functions*. Geophys. Res. Lett. 36.11. [available online]
[xxxii] Vrac, M. (2016) *Bias correction of precipitation through Singularity Stochastic Removal: Because occurrences matter.* Journal of Geophysical Research: Atmospheres, 121(10), 5091-6129 [available online]
[xxxiii] ISO. (2016). Petroleum and natural gas industries — Specific requirements for offshore structures — Part 1: Metocean design and operating considerations (ISO 19901-1:2015), p.15.
[xxxiv] Coles, S. (2001). An Introduction to Statistical Modelling of Extreme Values. Springer Series in Statistics.
[xxxv] IPCC. (2012). Managing the Risks of Extreme Events and Disasters to Advance Climate Change Adaptation. A Special Report of Working Groups I and II of the Intergovernmental Panel on Climate Change. [available online]
[xxxvi] Raynal-Villasenor, J. & al. (2014). *Estimation procedures for the GEV distribution for the minima*. Journal of Hydrology, 519, 512-522.
[xxxvii] Kysely, J. (2002). *Probability Estimates of Extreme Temperature Events: Stochastic Modelling Approach vs. Extreme Value Distributions.*.Studia Geophysica et Geodaetica, 46, 93–112. [available online]

Your contact:

contact@callendar.tech
www.callendar.tech

callendar